# Western Boundary Current Separation: Inferences from a Laboratory Experiment

PETER G. BAINES AND ROGER L. HUGHES*

*Division of Atmospheric Research, CSIRO, Aspendale, Victoria, Australia*

(Manuscript received 15 November 1994, in final form 13 October 1995)

ABSTRACT

Observations of a laboratory model of a western boundary current, and its separation and subsequent meandering, are described. The current is established by pumping fluid through a rotating channel that contains a topographic $\beta$ effect and continental slope topography. The observations are compared with a theoretical model of all three aspects of the current: the structure of the attached current, the process of separation, and the dynamics and path of the meandering jet. This model includes a viscous boundary layer for the attached current, with a thickness of order $[\nu/(dv_I/dy)]^{1/2}$, where $\nu$ is kinematic viscosity and $dv_I/dy$ is the velocity gradient of the inviscid (free slip) flow along the boundary.

Comparison between the observations and the model show that the attached boundary current is governed by potential vorticity conservation and the Bernoulli equation, and the pressure decreases along its length. The separation of this current from the sidewall is then caused by the minimum pressure level that is set by the downstream conditions in the tank, which forces the current into deeper water. The process is analogous to the separation of a boundary layer from a surface in an adverse pressure gradient in nonrotating flows. This process has implications for the separation of ocean boundary currents, where the details are more complex but clear analogies exist. Meanders in the separated current are qualitatively consistent with an inertial jet model, although detached eddies attributable to instability are also observed.

## 1. Introduction

The reason for the separation of western boundary currents from the coastlines of midlatitude ocean basins constitutes one of the "old chestnuts" of physical oceanography. Over the past few decades several mechanisms have been proposed, as described below, but the answer remains ambiguous (Fofonoff 1981; Veronis 1981). The wind-driven circulation in simple barotropic models (summarized by Stommel 1965) suggests that separation occurs at the latitude where the zonally averaged curl of the wind stress vanishes because fluid is driven toward the boundary equatorward of this latitude and away from it on the poleward side. There is some support for this on the average from observations of time-averaged wind stress in the North Atlantic (Leetmaa and Bunker 1978). However, there is considerable variability of the wind stress pattern with time, which contrasts with the relative constancy of the separation of the Gulf Stream at Cape Hatteras, and, if this mechanism *is* appropriate in the real ocean, it is not clear how it relates to the nonlinear local dynamics near the separation point. This process has been extended to a two-layer model by Parsons (1969) and Veronis (1973, 1981), where separation is interpreted as the surfacing of the lower layer at the coast.

In recent years this question has been addressed with numerical models. Although there are still uncertainties about the appropriate numerical details for modeling the ocean, such as the form of the boundary conditions, the determination of the separation point by the latitude of the vanishing of the mean wind stress curl has been shown to be questionable (Verron and Le Provost 1991).

The local dynamics of separation have previously been investigated with analytic and numerical models, and for a flat-bottomed ocean three possible (nonmutually exclusive) processes have been identified (Haidvogel et al. 1992). These are (i) separation by "detachment," which is essentially the process described by Parsons; (ii) separation by "vorticity crisis" (Pedlosky 1987), and (iii) separation by "adverse pressure gradient." The last of these is analogous to the well-known fluid dynamical process of separation of boundary layers from surfaces, and this is the process found to occur in the laboratory study described here.

The question of boundary current separation is investigated with a laboratory experiment in a rotating tank, where the flow is entirely barotropic. Here the flow is driven by a forced inflow and outflow at specific locations rather than by a simulated wind stress. The

* Additional affiliation: Department of Civil and Environmental Engineering, Parkville, Victoria, Australia.

*Corresponding author address:* Dr. Peter G. Baines, Division of Atmospheric Research, CSIRO, PB 1, Aspendale, VIC 3195, Australia.
E-mail: pgb@dar.csiro.au

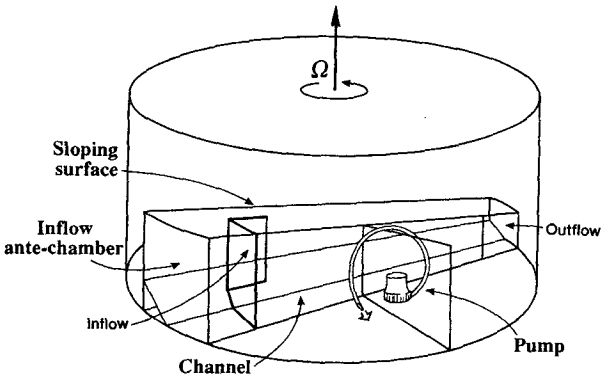


FIG. 1. Diagram of the rotating tank showing the submerged channel and the related geometry.

beta effect is simulated by a sloping bottom, and the sidewall may also have continental slope topography. The result is that a strong current forms that remains attached to the boundary over part of its path and then separates at a specific location and meanders toward the exit. The occurrence of separation, therefore, depends on the local dynamics (as it must also in the ocean), and these may be related to the external parameters of the experiment.

The plan of the paper is as follows. The experiment is described in section 2, and an outline and qualitative descriptions of the phenomena observed are given in section 3. Section 4 contains the theoretical development for the attached current including an inertial viscous boundary layer, the process of separation of the current from the wall and the reasons for it, the dynamics of the meandering path of the separated current, and the stability of the current. The sidewall boundary layer has a thickness of order $[\nu/(dv_I dy)]^{1/2}$, where $v_I$ is the inviscid velocity at the wall if free slip is assumed there, so that $dv_I/dy$ is the gradient of the downstream velocity just outside the boundary layer. In section 5, quantitative details of the observed flows are presented and compared with the predictions of section 4 with generally favorable results. The conclusions are summarized in section 6.

## 2. The experiment

A variety of different geometrical arrangements was tried in order to make a suitably controlled western boundary current, and after due experimentation the configuration shown in Fig. 1 was adopted. A transparent perspex channel (width 20 cm) with a rectangular cross section was constructed inside a circular tank (diameter 110 cm) on a turntable. The lid or upper surface of this channel was a movable plane surface, which could be repositioned so that the mean depth of the channel and the downchannel slope of the lid could be varied. In all experiments this lid was either horizontal or, more commonly, sloped downward from the inflow end to the exit end so that the depth in the channel decreased linearly along it. The mean depth was varied in the range 10–25 cm, and the difference in depths between the two ends of the channel was varied from zero to 10 cm. The fluid used was fresh (tap) water, which filled the entire channel so that there was no free surface.

The channel had an opening at each of the two ends, which permitted fluid to be pumped along it. A pressure difference between the two ends of the channel was achieved by a small centrifugal pump that pumped fluid from a reservoir adjoining the exit to a second reservoir adjoining the entrance to the channel. The entrance and exit were openings in a sidewall 10 cm wide adjacent to the channel ends (see Fig. 1), extending vertically over the full local depth of the channel. Fine wire mesh was placed across the entrance and exit in order to separate the two regions and to minimize the effect of any eddying motion in the upstream reservoir caused by the inflow from the pump, although these effects were arranged to be small anyway by positioning the pump. The level of fluid in the reservoirs was somewhat greater than the top of the channel.

Various forms of bottom topography could be inserted inside this channel. In most cases this topography took the form of a "continental slope" against the "western" wall, which is on the left-hand side looking downstream for the northern hemisphere (anticlockwise) rotation used in the experiment. This topography reached a height $h$ against this wall and decreased linearly to the bottom in a distance $a$ (Fig. 2b) with no variation along the channel. In most cases the slope width $a = 10$ cm, which is one-half the channel width. The channel cross section, therefore, varied down the channel due to the sloping lid and across the channel in the western half due to the bottom slope. If coordinates $x$ and $y$ are directed across and along the channel respectively, the local depth $D$ is a function of both $x$ and $y$.

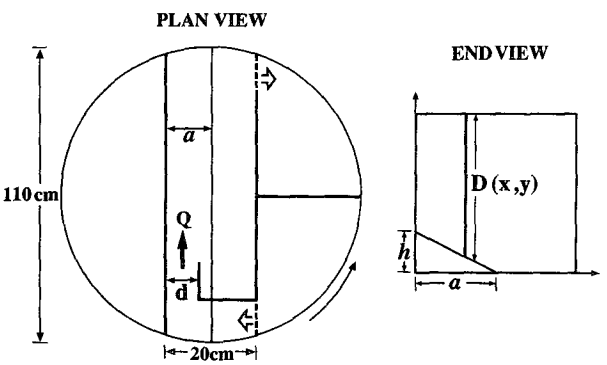


FIG. 2. (a) Plan view of the channel geometry. (b) End view of the channel geometry.

In some experiments with this channel, an $L$-shaped barrier, making an "antechamber" for the inflowing fluid with a narrow exit channel adjacent to the western boundary, was inserted (as shown in Figs. 1, 2a, 3). The initial reason for this barrier was to encourage the smooth formation of a western boundary current, but it was discarded for many of the experiments because it was not needed for this purpose.

Figure 2 shows a plan view and an end view of the channel, and indicates some of the major physical quantities. These are the total flux of fluid ($Q$) flowing down the channel; the Coriolis parameter, $f = 2\Omega$, where $\Omega$ is the angular velocity of the rotating turntable; the channel length $L$; the bottom topography dimensions ($h$ and $a$); the width ($d$) of the exit channel for the antechamber (if present); the depth of the channel at the inflow point ($D_i$); the viscosity $\nu$ and the two slopes, the across-channel slope, $\alpha = h/a$, and the along-channel slope, $\gamma = -\partial D/\partial y$. The slope $\gamma$ is positive and independent of $x$. The normal experimental procedure involved setting up the channel with the required geometrical configuration, filling the channel and reservoirs with fluid, and setting the tank in a state of constant rotation (with a typical rotation period of 4 s) for a period of approximately 30 minutes. This procedure established a state of rigid rotation in the channel and in the two reservoirs. The pump was then turned on, and an approximately steady state was established inside the channel within about 10 minutes. Two methods of flow visualization were used. In the first method dye was introduced into the upstream reservoir near the channel entrance. The flow was viewed from above using either a camera or a video camera, mounted on the turntable. The development of this dyed fluid with time showed the path of the fluid after it entered the channel and distinguished the inflowing fluid from the other relatively quiescent fluid in the channel. The second method used gave quantitative information about the velocity field. This method involved adding small neutrally buoyant polystyrene beads near the channel entrance (small enough to fit through the mesh at the entrance), illuminating the flow at one particular level, and observing the motion of the beads within the channel from above. This motion was recorded on videotape, and the Aspendale GFD laboratory's data acquisition system was utilized to obtain velocity fields and profiles. The velocity data were obtained by tracking beads over successive frames to obtain the fluid velocity field over the field of view of the camera. The flow was observed to be essentially barotropic with very little variation in the vertical (except possibly over sloping topography where $\alpha$ is large). So the flow observed at one level (above $h$) applied to all levels, excepting the flow within boundary layers on the top and bottom surfaces, which were thin and apparently inconsequential.

## 3. Observations of the character of the flow

After the commencement of the motion with steady external conditions $Q$ and $f$, an approximately steady flow state was reached in the channel after a period of several minutes (approximately 100 rotation periods). In many cases this flow was not completely steady and varied slowly with time about a mean configuration.

When the channel had a uniform rectangular cross section, with a horizontal upper surface and no bottom topography, with a rotation period of 4 s the flow down the channel was approximately uniform across it, apart from the divergence from the entrance and convergence to the exit, as shown in Fig. 3a. This flow pattern was similar to the mean flow that is observed when the same channel is not rotating, except that in the latter case the flow is turbulent with three-dimensional eddies. Rotation couples the motion in the vertical (the Taylor–Proudman effect), causing the flow to be effectively two-dimensional.

When the experiment is repeated with the channel lid tilted downward in the downstream direction, the initial flow (when the pump was turned on) was again uniform (approximately potential flow from entrance to exit), but the topographic beta effect caused topographic "Rossby" waves that transferred the flow toward the left-hand side of the channel (looking downstream). This effect was quite pronounced with even a very small slope of the lid and increased rapidly with it (Figs. 3b,c). This behavior resulted in a boundary current that was close to the left-hand boundary along its whole length, and at the end of the tank the current followed the boundary to the exit. A larger tilt of the lid resulted in a narrower current. This current carried most (typically 90%) of the transport of fluid down the channel, and the larger body of fluid occupying the remainder of the tank was relatively quiescent. However, the latter carried the remaining 10% or so of the transport in the form of a weak and apparently uniform barotropic flow (speed $< 1$ mm s$^{-1}$), as in Fig. 3a.

If "continental slope" bottom topography (as described in section 2) were introduced, the flow took a form such as that shown in Fig. 3d. The fluid (or most of it) again became organized into a boundary current when it entered the channel, stayed close to the wall for some distance down the channel, and then separated from the boundary to make its way to the exit by a more direct route. On the left-hand side of this separated current there was another region of relatively quiescent fluid. After separation the current generally developed stationary meanders, and some representative examples are shown in Figs. 3e and 3f.

In Fig. 3b the current contains a number of prominent eddies; and the ragged appearance of the boundary in Fig. 3d is due to a number of eddies and protuber-

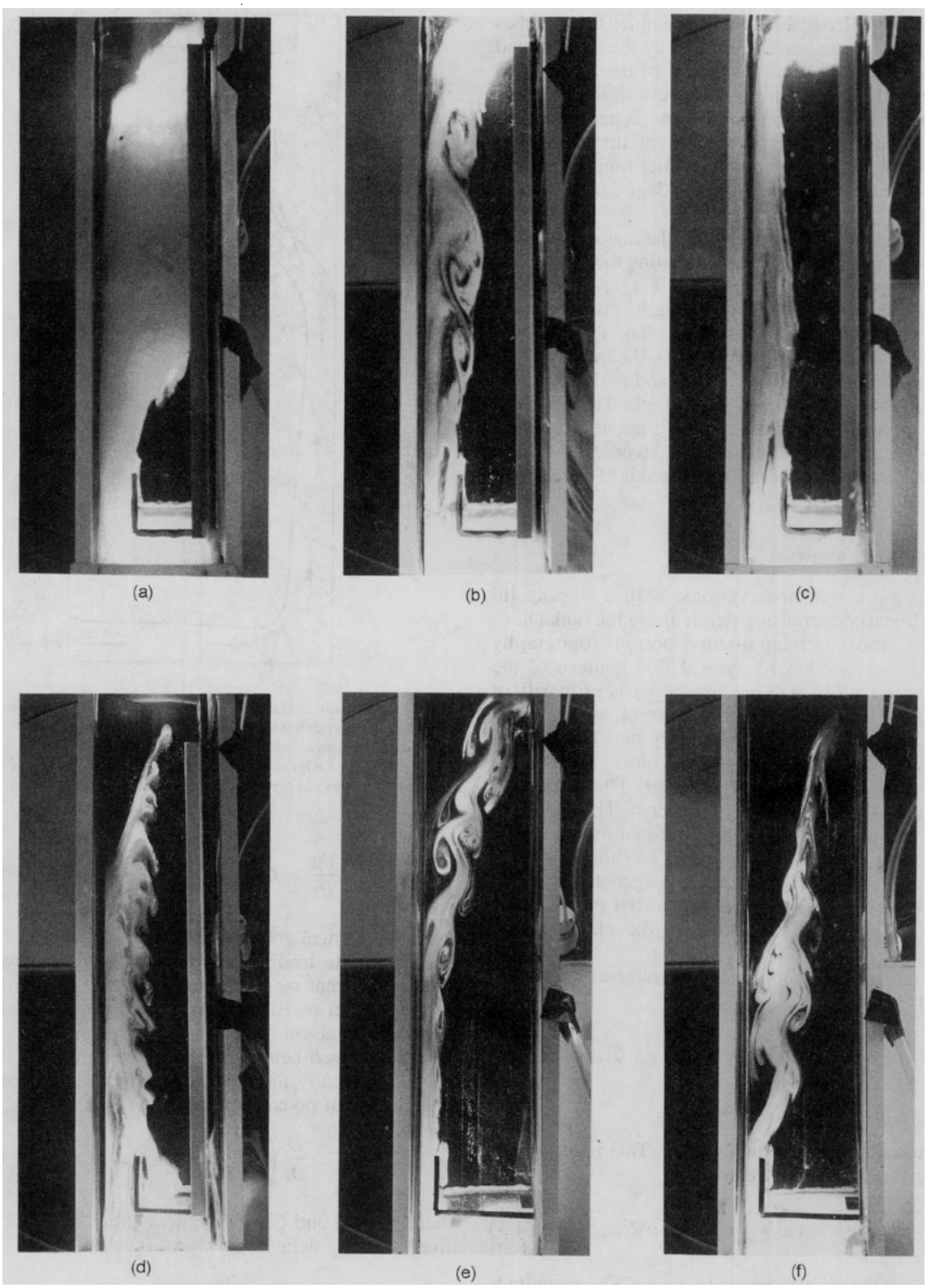


FIG. 3. Plan view of flow through the tank for various different depth configurations. Inflowing fluid is dyed white, and an antechamber with exit channel is present in all experiments here, although its effect is minimal in some cases. (a) Uniform depth $D = 21$ cm, $Q = 4$ L min$^{-1}$, $d = 6$ cm; (b) linearly decreasing depth down channel with $\gamma = 0.014$, $D_i = 21$ cm, uniform depth across it; (c) as in (b) but with $\gamma = 0.027$; (d) $D_i = 15$ cm, $\gamma = 0.055$, continental slope topography added in the left (western) half of the channel with $\alpha = 0.5$; (e) as in (d) but with $D_i = 22$ cm, $\gamma = 0.091$, $\alpha = 0.5$, and $d = 3$ cm; (f) as in (e) but with $D_i = 21$ cm, $\gamma = 0.055$.

ances of a smaller scale. In both examples these eddies are advected along and sheared out by the current, and they are attributed to an instability of the mean flow, as discussed below. Hence, they are transient features on an otherwise steady mean current. When meanders were observed on the separated current, they were similarly steady in the mean, with smaller time-dependent features on them (as seen in Figs. 3e, f) that are also attributable to instability.

From section 2, we may identify the major externally imposed dimensionless factors affecting the flow to be: the bottom slopes $\alpha$ and $\gamma$, and $\tilde{Q} = Q/fD_i^3$, the dimensionless flow rate. The tank length $L$ is not important in itself, provided only that it is long enough. Another significant term is the ratio $D_e/D_i$, where $D_e$ is the minimum depth in the channel and at the exit, and is related to $\gamma$ and $D_i$ by $D_e = D_i - \gamma L$. The observed maximum velocities were typically about 2 cm/sec, with a current width of about 5 cm. Hence, the *Rossby number* $R_0 = U/fl$ where $l$ is the width of the current is typically $2/15 \approx 0.13$, if $f = \pi$.

## 4. Theoretical analysis

From the above observations, with a sloping lid giving linearly decreasing depth along the tank (nonzero $\gamma$), and continental-slope bottom topography (nonzero $\alpha$), we have a typical flow pattern of the form shown in Fig. 4. This flow consists primarily of a relatively narrow barotropic current, which is attached to the "western" boundary and then subsequently separates to make its way more directly, but with possible meanders, to the exit. The remaining fluid in the tank is relatively quiescent. This behavior suggests that the most appropriate theoretical model to describe these observations is a "hose model," consisting of a relatively thin quasigeostrophic current. However, it is appropriate to first consider the equations governing the flow in the channel as a whole.

The equations of motion of a homogeneous viscous fluid are

$$\frac{D\mathbf{u}}{Dt} + \mathbf{f} \times \mathbf{u} = -\frac{1}{\rho}\nabla p + \nu\nabla^2\mathbf{u}, \qquad (4.1)$$

$$\nabla \cdot \mathbf{u} = 0, \qquad (4.2)$$

in the usual notation, with $\mathbf{f} = 2\Omega\mathbf{z}$. Taking the curl of (4.1) gives the vorticity equation

$$\frac{D\omega}{Dt} = (\omega + f)\cdot\nabla\mathbf{u} + \nu\nabla^2\omega, \qquad (4.3)$$

where $\omega$ is the relative vorticity vector. The magnitude of $|\omega/f|$ is approximately equal to the Rossby number $R_0$ as defined above. If this number is small, as in these experiments, then outside the boundary layers (4.3) gives that

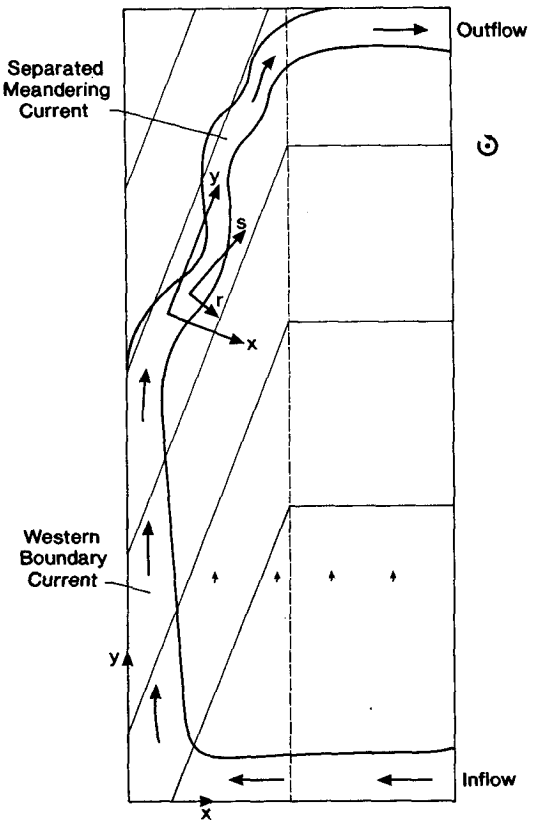


FIG. 4. Schematic diagram of the horizontal flow pattern in the tank showing the coordinate systems for the attached and meandering current, and the typical bottom contours (shallowest depth is at upper left). Outside the designated current the fluid is relatively stagnant, but weak velocities are present with the directions shown.

$$\frac{\partial\mathbf{u}}{\partial z} = O(R_0)\left(\frac{\partial\mathbf{u}}{\partial x}, \frac{\partial\mathbf{u}}{\partial y}\right), \qquad (4.4)$$

so that the vertical gradients are negligible and the flow is barotropic to leading order in $R_0$. For the attached boundary current we therefore envisage a flow with a barotropic interior, Ekman layers on the top and bottom boundaries, and a sidewall boundary layer, with structure as discussed below. Integrating the inviscid form of (4.3) vertically then gives the familiar equation of conservation of potential vorticity

$$\frac{D}{Dt}\left(\frac{\zeta + f}{D(x, y)}\right) = 0, \qquad (4.5)$$

where $f = 2\Omega$ and $\zeta$ is the vertical component of (relative) vorticity defined by

$$\zeta = \frac{\partial v}{\partial x} - \frac{\partial u}{\partial y}, \qquad (4.6)$$

where $u$ and $v$ are the vertically averaged velocity components in the $x$ and $y$ directions respectively. This inviscid

interior flow is governed by the volume flux $Q$ and the geometry of the tank. We next investigate its character and then discuss the effects of the viscous boundary layers.

*a. The attached western boundary current: inviscid model*

With a flow configuration as shown in Fig. 2, the depth in the left-hand side of the channel has the form

$$D(x, y) = D_0(y) + \alpha x,$$

where

$$D_0(y) = D_i - h - \gamma y \tag{4.7}$$

with the western boundary at $x = 0$. Further, when the flow is steady, this low Rossby number flow must be barotropic. The vertically integrated continuity equation has the form

$$\nabla\cdot(D\mathbf{u}) = 0 \tag{4.8}$$

so that we may define a streamfunction $\psi$ by

$$u = -\frac{1}{D}\frac{\partial\psi}{\partial y}, \quad v = \frac{1}{D}\frac{\partial\psi}{\partial x}. \tag{4.9}$$

Equation (4.5) then integrates to

$$\frac{\zeta + f}{D} = F(\psi), \tag{4.10}$$

where $F$ is some arbitrary function, representing conservation of potential vorticity along a streamline. For steady state we also have the Bernoulli relationship

$$\frac{1}{2}(u^2 + v^2) + \frac{p}{\rho} = G(\psi), \tag{4.11}$$

where $p$ is the vertically averaged pressure and for steady flow $F(\psi) = dG/d\psi$ (e.g., see Gill 1982, §7.10).

In the experiment, we may regard the inflowing fluid as coming from a large region with effectively uniform potential vorticity and zero relative vorticity (see next section). Consequently, for the fluid in a boundary current we have

$$F(\psi) = \text{const} = \frac{f}{D_i}. \tag{4.12}$$

We must also have $|\partial u/\partial y| \ll |\partial v/\partial x|$ in the boundary current so that (4.10) becomes

$$\frac{\partial v}{\partial x} = f\left(\frac{D}{D_i} - 1\right). \tag{4.13}$$

If there is no antechamber, the width of the current is determined by the dynamics. The boundary condition at the outer edge is then

$$v = 0 \quad \text{at} \quad x = x_b(y), \tag{4.14}$$

where $x_b$ is an as yet unknown variable that denotes the width of the current. Equation (4.13) then integrates to

$$v(x, y) = f(x_b - x)\left(1 - \frac{D_0(y) + \alpha(x + x_b)/2}{D_i}\right), \tag{4.15}$$

where $D_0(y)$ is the depth of the channel at $x = 0$. In the boundary current of Fig. 3, if $Q_b$ is the total flux of fluid in the current (where $Q_b \leqslant Q$), we have

$$Q_b = \int_0^{x_b} Dv\,dx, \tag{4.16}$$

which is a constant independent of $y$. If we define the dimensionless quantities

$$A = \frac{D_0(y)}{D_i}, \quad X_b = \frac{\alpha x_b(y)}{D_i},$$
$$\left(\hat{Q}, \hat{Q}_b\right) = \frac{\alpha^2}{f D_i^3}(Q, Q_b), \tag{4.17}$$

substituting (4.15) into (4.16) gives

$$X_b^4 - \frac{4}{3}(1 - 3A)X_b^3 - 4A(1 - A)X_b^2 + 8\hat{Q}_b = 0, \tag{4.18}$$

which determines the width and structure of the current. For any particular $y$, (4.18) has two positive roots for $X_b$ of which the smaller is the physically significant one in the present context. If $\hat{Q}_b \ll 1$, this root is given approximately by a balance between the last two terms so that

$$X_b \approx \left(\frac{2\hat{Q}_b}{A(1 - A)}\right)^{1/2}. \tag{4.19}$$

Since $A$ is initially in the range $0.5 < A < 1$ and decreases with increasing $y$, $X_b$ decreases and the current initially becomes thinner. The largest velocity is found next to the sidewall. As shown in Fig. 6, for the conditions of these experiments the velocity decreases monotonically with distance $x$ from the wall, in an approximately linear fashion to zero at the edge of the current. Both the velocity and the anticyclonic shear increase in the downstream $y$ direction as the depth decreases, according to (3.13). Properties of boundary currents of this form have been studied by Hughes (1985, 1986). If we denote the streamfunction for this inviscid flow by $\psi_I$, we may define

$$\psi_I(x, y) = \int_0^x Dv\,dx, \tag{4.20}$$

where $\psi_I(x_b, y) = Q_b$.

If an antechamber with exit channel of width $d$ is present where $d < x_b$, as in Fig. 3, the width of the current is then specified as $d$ and (4.13) integrates to give

$$v(x, y) = v(0, y) + f\left[-\left(1 - \frac{D_0(y)}{D_i}\right)x + \frac{\alpha x^2}{2D_i}\right]. \tag{4.21}$$

Then $v(0, y)$ is determined from $Q_b$ by

$$Q_b = \int_0^d Dv dx. \tag{4.22}$$

*b. The attached western boundary current: the viscous boundary layer*

The Ekman layers have thickness $(\nu/f)^{1/2} \sim 0.1$ cm, and the suction velocity into them is $w \sim 0.5\ (\nu/f)^{1/2}\zeta$, which is typically 0.02 cm s$^{-1}$. The flow into these layers is returned to the interior by a corresponding Stewartson layer [thickness $(\nu D/f)^{1/3}$] on the sidewall (e.g., Greenspan 1968), which produces a spindown effect. This spindown reduces the anticyclonic shear of the current, and hence its velocity, resulting in a net drag. With a typical current speed of 2 cm s$^{-1}$, in a distance of 50 cm this gives an inflow into each Ekman layer of 0.5 cm of the fluid column, which is a small part of the total depth. Hence, this circulation is weak, and the effect is small if not negligible.

There is an additional boundary layer on the side wall due to the no-slip condition there, and this is our principal concern here. Adding the viscous terms, (4.5) becomes (Gill 1982)

$$\frac{D}{Dt}\left(\frac{\zeta + f}{D(x, y)}\right) = \frac{\nu}{D}\nabla^2\zeta. \tag{4.23}$$

Eliminating the vorticity in favor of the streamfunction defined by (4.9) yields, in steady-state form

$$\begin{aligned}\frac{1}{D}&\left(-\frac{\partial\psi}{\partial y}\frac{\partial}{\partial x} + \frac{\partial\psi}{\partial x}\frac{\partial}{\partial y}\right)\left(\frac{\partial}{D\partial x}\left(\frac{1}{D}\frac{\partial\psi}{\partial x}\right)\right.\\ &\left. + \frac{\partial}{D\partial y}\left(\frac{1}{D}\frac{\partial\psi}{\partial y}\right)\right) - \frac{1}{D^3}\left(\frac{\partial}{\partial x}\left(\frac{1}{D}\frac{\partial\psi}{\partial x}\right)\right.\\ &\left. + \frac{\partial}{\partial y}\left(\frac{1}{D}\frac{\partial\psi}{\partial y}\right) + f\right)\left(-\frac{\partial\psi}{\partial y}\frac{\partial D}{\partial x} + \frac{\partial\psi}{\partial x}\frac{\partial D}{\partial y}\right)\\ &= \frac{\nu}{D}\nabla^2\left(\frac{\partial}{\partial x}\left(\frac{1}{D}\frac{\partial\psi}{\partial x}\right) + \frac{\partial}{\partial y}\left(\frac{1}{D}\frac{\partial\psi}{\partial y}\right)\right).\end{aligned} \tag{4.24}$$

Within the boundary layer of thickness $\delta \approx 0.5$ cm and with $\alpha \approx 0.5$, $D > 10$ cm, we have

$$\left|\frac{\partial}{\partial y}(\psi, v)\right| \ll \left|\frac{\partial}{\partial x}(\psi, v)\right|,$$

$$\left|\frac{v}{D}\frac{\partial D}{\partial x}\right| \ll \left|\frac{\partial v}{\partial x}\right|, \left|\frac{1}{D}\frac{\partial v}{\partial x}\right| \ll \left|\frac{\partial^2 v}{\partial x^2}\right|. \tag{4.25}$$

Employing these approximations in (4.24), we obtain

$$\underbrace{\left(-\frac{\partial\psi}{\partial y}\frac{\partial}{\partial x} + \frac{\partial\psi}{\partial x}\frac{\partial}{\partial y}\right)\frac{\partial^2\psi}{\partial x^2}}_{\text{I}} \underbrace{-\frac{f}{D}\left(-\frac{\partial\psi}{\partial y}\frac{\partial D}{\partial x} + \frac{\partial\psi}{\partial x}\frac{\partial D}{\partial y}\right)}_{\text{II}} = \nu D\frac{\partial^4\psi}{\partial x^4}. \tag{4.26}$$

Of the two terms on the left-hand side, term I denotes advection of relative vorticity $\zeta$, and term II the stretching of "planetary" vorticity $(f/D)$. If

$$\frac{f\alpha}{D} \ll \frac{v}{\delta^2}, \quad f \ll \frac{\partial v}{\partial x}, \tag{4.27}$$

term I dominates term II. This is the case within the boundary layer so that term II may be neglected there relative to term I [for a description of the dynamics when the inequalities of (4.27) are reversed and term I is negligible, see Hughes (1993)]. We define

$$\psi = \psi_I + \psi_V, \quad \mathbf{u} = \mathbf{u}_I + \mathbf{u}_V, \quad \zeta = \zeta_I + \zeta_V, \tag{4.28}$$

where $\psi_I$, $\mathbf{u}_I$, and $\zeta_I$ refer to the inviscid solution of section 4a, and $\psi_V$, $\mathbf{u}_V$, and $\zeta_V$ denote the viscous modification. We assume that $\delta$ is sufficiently small so that

$$\mathbf{u}_I = \text{const}, \quad \zeta_I = 0 \tag{4.29}$$

in the boundary-layer. Thus, (4.26) with assumption (4.27) may be integrated directly with respect to $x$ to give

$$-\frac{\partial\psi}{\partial y}\frac{\partial^2\psi}{\partial x^2} + \frac{\partial\psi}{\partial x}\frac{\partial^2\psi}{\partial y\partial x} = \nu D\frac{\partial^3\psi}{\partial x^3} + P(y), \tag{4.30}$$

where the function of integration is

$$P(y) = \frac{1}{2}\frac{\partial}{\partial y}(D_0(y)v_I(0, y))^2. \tag{4.31}$$

This equation is similar to that for a Blasius boundary layer on a flat plate (e.g., see Batchelor 1967) except that here the downstream pressure gradient is negative due (in part) to the effect of rotation on the flow, resulting in the negative term $P(y)$.

To solve this equation, we write

$$\psi = W(y)(x + \delta(y)\Psi(\xi)), \tag{4.32}$$

where

$$W(y) = D_0(y)v_I(0, y), \quad \xi = x/\delta(y), \tag{4.33}$$

and $\delta$ represents the width of the boundary layer. The total velocity $v$ in the boundary layer is then given by

$$v = \frac{1}{D}\frac{\partial\psi}{\partial x} = v_I\left(1 + \frac{d\Psi}{d\xi}\right). \tag{4.34}$$

Substituting (4.32) into (4.30) then gives

$$\frac{d^3\Psi}{d\xi^3} + (1+B)(\xi+\Psi)\frac{d^2\Psi}{d\xi^2} - \left(\frac{d\Psi}{d\xi}\right)^2 - 2\frac{d\Psi}{d\xi} = 0, \quad (4.35)$$

where

$$B = \frac{W}{\delta}\frac{d\delta/dy}{dW/dy}, \quad \delta^2 = \frac{\nu D_0(y)}{dW/dy}. \quad (4.36)$$

The boundary conditions on (4.35) are

$$\Psi = 0, d\Psi/d\xi = -1 \quad \text{at} \quad \xi = 0 \quad (4.37)$$

$$\Psi \to \text{const} \quad \text{as} \quad \xi \to \infty. \quad (4.38)$$

Equation (4.35) was solved subject to (4.37), (4.38) by numerical integration using a fourth-order Runge–Kutta integration procedure. The resulting velocity profiles $v/v_I$ in the boundary layer are shown in Fig. 5. The profiles are monotonic and reach 75% of their inviscid value at $\xi = 1$ ($x = \delta$). They are only weakly dependent on $B$, provided that $B$ is significantly greater than $-1$.

From (4.36) the boundary layer width $\delta$ may be written as

$$\delta^2 = \nu/(dv_I/dy - \gamma v_I/D_0). \quad (4.39)$$

For these experiments $|\gamma v_I/D_0| \ll |dv_I/dy|$ so that

$$\delta \approx \left(\nu/\frac{dv_I}{dy}\right)^{1/2}. \quad (4.40)$$

The width of the boundary layer is therefore determined by the acceleration of the external flow produced by the downstream pressure gradient. In the limit $dv/dy \to 0$, $\delta \to \infty$. This result is consistent with the boundary layer in the absence of a downstream pressure gradient, which takes the Blasius form. The latter never reaches a steady state but continues to widen to infinity with distance downstream. Note that the downstream pressure gradient, which keeps the boundary layer at finite width, is applied by the dynamics of the inertial boundary current in which the viscous boundary layer occurs. The parameter $B$ in (4.36) may be expressed as

$$B = \frac{v_I}{\nu}\frac{d}{dy}\left(\frac{1}{2}\delta^2\right) = \frac{1}{2}\left(1 - \frac{D_0}{(D_i - \alpha x_b/2)}\right) \quad (4.41)$$

so that its values are generally small and positive and, therefore, are not very significant.

The external pressure gradient causes positive relative vorticity to be generated at the wall (Morton 1984). This generation tends to counteract the production of negative relative vorticity from the compression of the water column in the current as it flows along the tank. If they balance, there is no persistent tendency for the thickness of the boundary layer to increase due to diffusion, as occurs in the Blasius boundary layer.

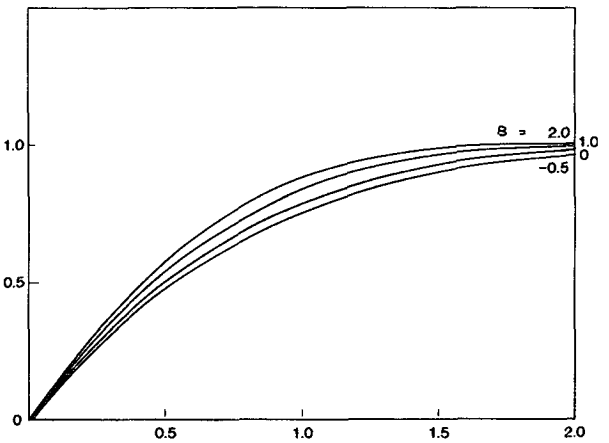


FIG. 5. Velocity profiles $v/v_I$ (ordinate) in the boundary layer as a function of $\xi = x/\delta$ (abscissa) for various values of the parameter $B$ [see (4.36), (4.41)]. Note that the sensitivity to the value of $B$ is slight.

*c. The process of separation*

Noting that the viscous boundary layer required to satisfy the no-slip condition at the wall is much thinner than the inertial boundary current, we return to the inviscid model of the current in section 4a. Here the steady-state equations have been integrated in the downstream direction, and are valid provided that the conditions (boundary, topography, etc.) remain uniform and that no signals or disturbance propagate upstream from the downstream end. No change in this behavior is predicted by this viscous correction. But in Figs. 3d–f the boundary current is observed to separate from the sidewall and, while maintaining its identity, makes its way to the exit by a more direct route than in Figs. 3b and 3c, between two regions of relatively quiescent fluid. Clearly, the downstream conditions imposed by the end of the tank and particularly the exit region are responsible for this separation, and the overall flow pattern is highly nonlinear.

If we assume that the flow has the form shown in Fig. 4, where for small $R_0$ the current is in approximate geostrophic balance, then the difference in pressure across the current at the exit is

$$\Delta p_e = \rho \int fu dy = \rho f Q_b/\overline{D_e}, \quad (4.42)$$

where $\overline{D_e}$ is the flow-weighted mean depth across the exit. Similarly, the difference in pressure across the current when attached to the boundary, from the inviscid model of section 4a, is

$$\Delta p = p(x_b) - p(0) = \rho \int_0^{x_b} fv dx = \rho f Q_b/\overline{D(y)}, \quad (4.43)$$

where $D(y)$ is the flow-weighted mean depth across the current and $\Delta p$ is positive. Since the pressure in the stagnant region on the right of the current is approximately constant, (4.43) shows that $\Delta p$ increases with increasing $y$ because the pressure at the wall decreases. If the current remains attached to the sidewall, $\Delta p$ will increase as $\overline{D(y)}$ decreases and then decrease as $\overline{D(y)}$ increases to $\overline{D_e}$. This implies that the pressure at the wall passes through a minimum. However, it is customary in fluid mechanics for flow along boundaries in opposing pressure gradients to separate from them if this separation reduces the variation in pressure. This property has been observed in numerical studies of western boundary currents in rotating fluids by Haidvogel et al. (1992). (It may be generalized by noting that in unforced mathematical "elliptic" systems for $p$, extreme values of $p$ are avoided.) If this criterion is applied here, we would expect separation to occur when $\Delta p$ increased to a value slightly beyond $\Delta p_e$ as given by (4.42), to avoid the adverse pressure gradient at the wall with consequent deceleration and even reversed flow farther downstream. This would cause the current to separate from the wall, as observed, and move out into deeper water so that the pressure difference across it is less than that given by (4.43). The flow in the region to the left of the separated current is observed to be relatively stagnant, but weak circulation with flow at the wall toward the separation point is noticed, consistent with this interpretation. This criterion implies that for the current to remain attached we must have

$$\Delta p \leqslant \Delta p_e \tag{4.44}$$

so that $\overline{D(y)} \geqslant \overline{D_e}$. Thus, the criterion for separation is $\overline{D(y)} = \overline{D_e}$. For practical purposes we approximate $\overline{D_e}$ by the mean depth at the exit, $D_m$. The addition of the viscous boundary layer of section 4b to this model does not affect the pressure at the wall in the attached current so that this criterion is largely unaffected. A quantitative test through comparison with observations is given in the next section.

### *d. The separated current: jet model*

The attached current has zero velocity on both sides (at the wall because of the no-slip condition and the viscous layer). Once separation has occurred, the current flows over the slope to deeper water and its structure varies while still maintaining zero velocity on each side. It adjusts to a consequent excess or deficit of vorticity by undergoing meanders. The full modeling of this process including structural changes to the current is extremely cumbersome. However, since the separated current is observed to maintain its identity, its behavior may be modeled by regarding it as a free inertial current or jet, as described by Robinson and Niiler (1967). We again assume that the horizontal flow pattern is independent of depth and also that the flow in the across-current direction is in gradient wind balance. Adopting curvilinear coordinates $(r, s)$ across and along the current, as shown in Fig. 4, with $U$ and $V$ as the velocity components in the $r$ and $s$ directions, respectively, the equations of motion may be written

$$-\kappa V^2 - fV + \frac{1}{\rho}\frac{\partial p}{\partial r} = 0, \tag{4.45}$$

$$U\frac{\partial V}{\partial r} + V\frac{\partial V}{\partial s} + w\frac{\partial V}{\partial z} + \kappa UV + fU + \frac{1}{\rho}\frac{\partial p}{\partial s} = 0, \tag{4.46}$$

where $\kappa$ is the curvature of the stream. Here $\kappa$ is a function of $s$ but is assumed to be independent of $r$. The vorticity equation corresponding to (4.13) (omitting $\partial U/\partial s$) is then

$$\frac{\dfrac{\partial V}{\partial r} + \kappa V + f}{D(r, s)} = C(r), \tag{4.47}$$

where $C$ is constant along a streamline. For the right-hand side of the current we may expect that $C = f/D_i$ as in (4.12), but the left-hand side has been affected by the injection of potential vorticity from the sidewall into the boundary layer. For this reason an integrated approach to the path of the current is appropriate. Multiplying (4.47) by DV and integrating across the current gives

$$\kappa\langle V^2\rangle + f\langle V\rangle = \langle CDV\rangle, \tag{4.48}$$

where

$$\langle V^2\rangle \equiv \int_{-\infty}^{\infty} V^2 dr, \quad \text{etc.} \tag{4.49}$$

Whereas for the attached boundary current the change in depth is manifested in changing shear, for the separated current the shear term vanishes on integration, and the changing depth is manifested in changing current curvature. This property has been used by Robinson and Niiler (1967) to calculate current paths under various conditions. Since $\langle DV\rangle = Q_b$, $\langle V\rangle = Q_b/\bar{D}(s)$, where again $\bar{D}$ is the flow-weighted mean depth across the current, (4.48) may be written

$$(\kappa - \kappa(0))\langle V^2\rangle + fQ_b/\bar{D}(s) = fQ_b/\bar{D}(0), \tag{4.50}$$

where $\kappa(0)$ is the curvature at a chosen origin for $s$ where $\bar{D} = \bar{D}(0)$. If we suppose that $\kappa(0) = 0$, then (4.50) shows that $\kappa$ remains zero if $\bar{D}(s)$ remains equal to $\bar{D}(0)$. Hence, the path of the current is straight, along a line of constant depth. However, if the current is not initially aligned in this direction, it will oscillate or meander about it, with $\kappa$ positive in deeper water and negative in shallower. The only straight paths (i.e., with zero curvature) are those that follow the contours of constant depth so that $\bar{D}(s) = \bar{D}(0)$.

If we take Cartesian coordinates $(X, Y)$ with the $Y$ axis aligned along the constant depth contours and consider small departures from this path, the linearized form of (4.50) with $\kappa \approx d^2X/dY^2$, $\kappa(0) = 0$ becomes

$$\langle V^2 \rangle \frac{d^2X}{dY^2} + \frac{f Q_b}{\bar{D}(0)^2} \frac{d\bar{D}}{dX} X = 0. \qquad (4.51)$$

Hence, small disturbances have a wavelength given by

$$L = 2\pi \left( \frac{\langle V^2 \rangle \bar{D}^2}{f Q_b dD/dX} \right)^{1/2}, \qquad (4.52)$$

where $d\bar{D}/dX = dD/dX = (\alpha^2 + \gamma^2)^{1/2}$, and if we define the width of the current $l$ by $\langle V^2 \rangle = Q_b^2/\bar{D}^2 l$, then

$$L = 2\pi \left( \frac{Q_b}{fl dD/dX} \right)^{1/2}. \qquad (4.53)$$

It would appear that a smooth junction between the boundary current model and the separated jet model is not possible because of the different structures of the two forms of the current. Nevertheless, one may regard the state of the boundary current immediately before separation as an approximate initial condition for the separated current, with zero curvature and alignment along the wall, in order to obtain magnitudes. The initial conditions for (4.51) are then

$$X = 0, \quad \frac{dX}{dY} = -\frac{\gamma}{\alpha} \quad \text{at} \quad Y = 0, \qquad (4.54)$$

so that the solution is

$$X = -\frac{\gamma}{\alpha} \frac{L}{2\pi} \sin 2\pi Y/L, \qquad (4.55)$$

yielding meander amplitudes of $\gamma L/2\pi\alpha$. Since $\gamma/\alpha \approx 0.2$, $dX/dY$ is small and the linearization would appear to be justified.

## 5. Quantitative observational results

We now compare the theoretical picture of the preceding section with detailed observations, addressing each of the same three parts of the flow in turn.

### *a. The attached current*

We describe the properties of the first part of the current, where it is attached to the boundary. As described in section 3, the boundary current carries typically 90% of the transport, and it is necessary to measure the flux $Q_b$ in this current in order to be able to compare the models of section 4 with the observations. This value of $Q_b$ is obtained from observed velocity profiles in the current.

Figure 6 shows a representative example of observed velocity profiles in the boundary current in an experiment where there is no antechamber, compared with velocity profiles from the inviscid model of section 4a and incorporating the boundary layer model of section 4b, using the observed value of $Q_b$, which equals $0.91Q$ for this flow. The observed velocity profiles were obtained by tracking small beads in the flow illuminated at a level near middepth and using these to construct velocities. The profiles shown in Fig. 6 are taken from the range 22–41 cm from the upstream end of the tank, and are all within the range where the current is attached to the boundary. The observed profiles in Figs. 6a and 6b are reasonably close to those of the inviscid profiles (shown dashed) outside the boundary layer (i.e., at distances greater than 1 cm from the sidewall) except that the current is a little wider than predicted. The latter is attributed to eddies at the edge of the current of the form seen in Fig. 3d. Farther downstream the comparison is similar except that the maximum in the velocity profile is reduced compared with that from the viscous model. The relatively small thickness of the boundary layer makes it difficult to observe the velocities close to the wall accurately by this method, but in spite of the aforementioned differences there is general agreement between experiment and theory, which implies that the flow is consistent with the dynamics described in the previous section.

The form of the small-scale eddies shown in Fig. 3d resembles Kelvin–Hemholtz billows, and suggests that these features are due to instability of the mean flow. However, the inviscid flow described in section 4a is stable and supports two neutral modes that are centered on the edge of the current. These modes are due to the discontinuity in potential vorticity at the edge of the current and the potential vorticity gradient just outside it, and one mode propagates with the current and the other against it. However, if one takes a simple approximation to a viscous profile shown in Fig. 6, inviscid disturbances to this profile are unstable. This instability occurs because waves in this inner region may interact with waves on the current edge (e.g., see Baines and Mitsudera 1994). These calculations are straightforward and are not described here. They do indicate the nature of the process that causes the eddies, but a more detailed study incorporating viscosity is required.

### *b. Separation*

The above comparison shows that the inviscid model plus the steady viscous boundary layer provide a good description of the attached boundary current. However, when the current reaches the separation point, the current detaches and moves "offshore," and the model becomes inadequate. The discussion in section 4c implies that separation occurs when the mean depth in the current $\overline{D(y)} = \overline{D_e}$, and this mechanism is independent of whether the form of the current is given by (4.15) or (4.21). A large number of experimental runs covering a wide range of conditions have been carried out

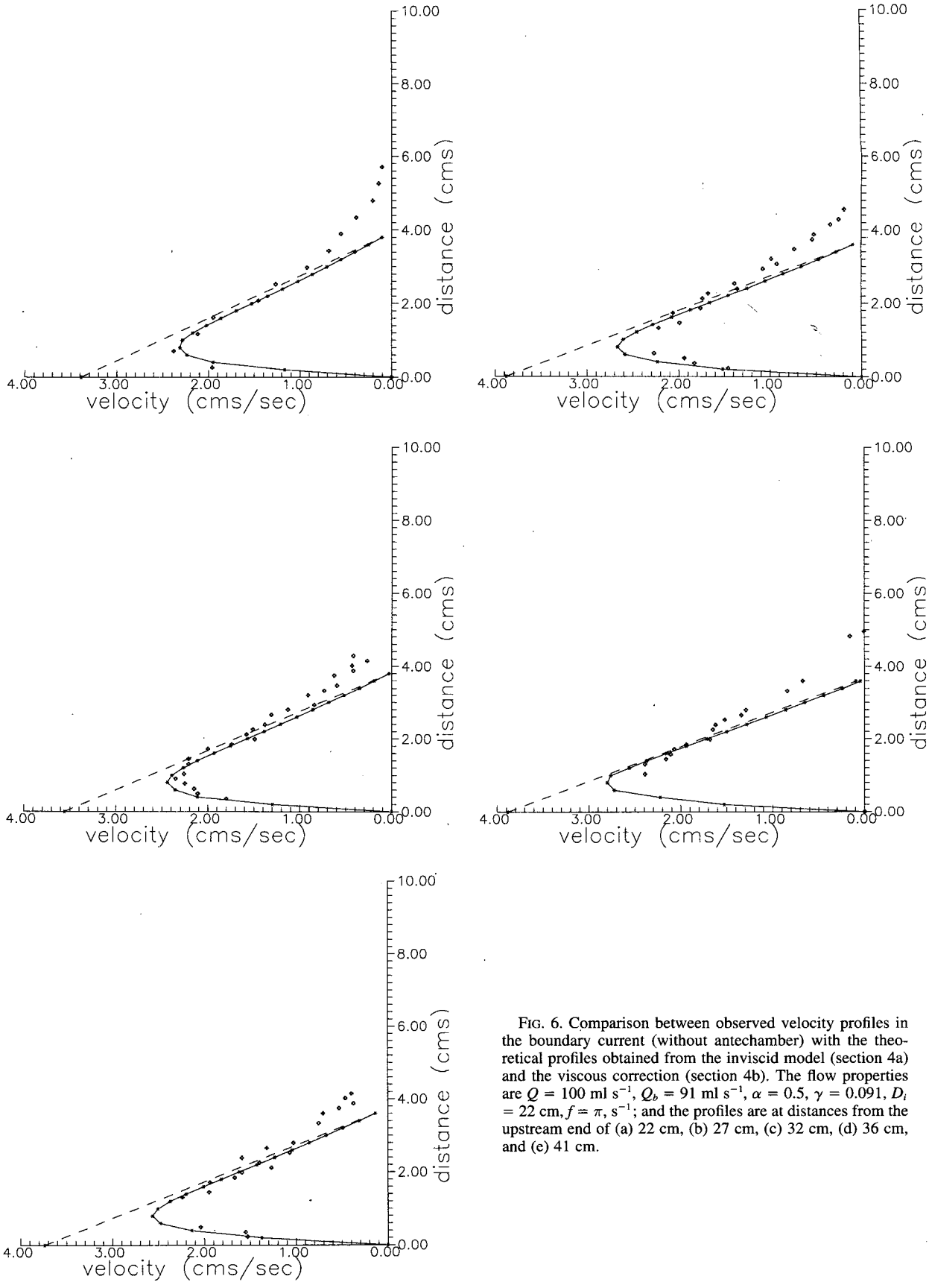


FIG. 6. Comparison between observed velocity profiles in the boundary current (without antechamber) with the theoretical profiles obtained from the inviscid model (section 4a) and the viscous correction (section 4b). The flow properties are $Q = 100$ ml s$^{-1}$, $Q_b = 91$ ml s$^{-1}$, $\alpha = 0.5$, $\gamma = 0.091$, $D_i = 22$ cm, $f = \pi$, s$^{-1}$; and the profiles are at distances from the upstream end of (a) 22 cm, (b) 27 cm, (c) 32 cm, (d) 36 cm, and (e) 41 cm.

to observe this separation and the factors determining its location, and to test the criterion of section 4c. We may take the depth $D_s$ of the fluid at the wall at the point of separation, as a measure of the location of this separation point, and scale this by the mean depth $D_m$ of the fluid at the exit of the tank. In all of these experiments the forms of the profiles are similar to those shown in Fig. 6, but these have not been computed in every case. Instead, for comparison with the theoretical predictions of section 4c we use $D_s$ and $D_m$ as surrogates for $\overline{D(y)}$ and $\overline{D_e}$, respectively. Here $D_s$ is clearly less than $\overline{D(y)}$ by an amount that depends on $\alpha$, but $D_m$ may be taken to be a reasonable approximation to $\overline{D_e}$.

The observed values of $D_s/D_m$ for a number of experiments are shown in Fig. 7 as a function of the parameter $\hat{Q}$ over four decades of values, and for a range of values of $\alpha$ and $\gamma$. In all of these cases the continental shelf topography was 10 cm wide, and the boundary current was wholly located over it. This diagram shows that $D_s$ is generally very close to $D_m$ with a tendency to be somewhat smaller. In fact, there is an evident trend for $D_s/D_m$ to decrease as $\alpha$ increases, which is consistent with the expectations from the theory since $\overline{D(y)}/D_s$ increases with $\alpha$. There is no apparent dependence of $D_s/D_m$ on $\gamma$. Although most experiments were carried out with $f = \pi$ (rotation period 4 s), $f$ was also varied in the range from 0.125 to $2\pi$, with no noticeable effect on the location of separation.

The above criterion for separation has been kept simple for clarity, and the situation is slightly more complicated because $Q_b$ is not equal to $Q$, due to a weak, approximately uniform flow in the region outside the boundary current. It is not possible to allow for this quantitatively here because $Q_b$ was only measured in a few representative cases, but the differences and the inferred consequences are small.

### c. *The separated current*

As the examples of Figs. 3d–f show, the mean path of the separated current is consistent with the expectation of section 4d that it follow the contours of constant depth toward the exit, with meanders superimposed. The amplitude of the observed meanders is approximately 1.3 cm (2.6 cm crest to trough), as predicted by the theory of section 4d. The wavelength of the observed meanders is of the order of 20 cm, with a tendency to increase with increasing $Q$, which is consistent with the predicted values of the free jet model. However, detailed quantitative comparison with theory has not been attempted, partly because the path of the current is complicated by the presence of smaller eddies and "prominences" on the meanders (see Figs. 3e, f for examples), which are attributed to shear flow instability that is localized on the meanders in many cases.

Considerable variety was observed in the flow patterns with these meanders and smaller features, most of which could be qualitatively attributed to a combination of the dynamical factors described in section 4. One particular observed phenomenon is worthy of note, and an example is shown in Fig. 3f. Here the eddying activity is concentrated in one particular region of the

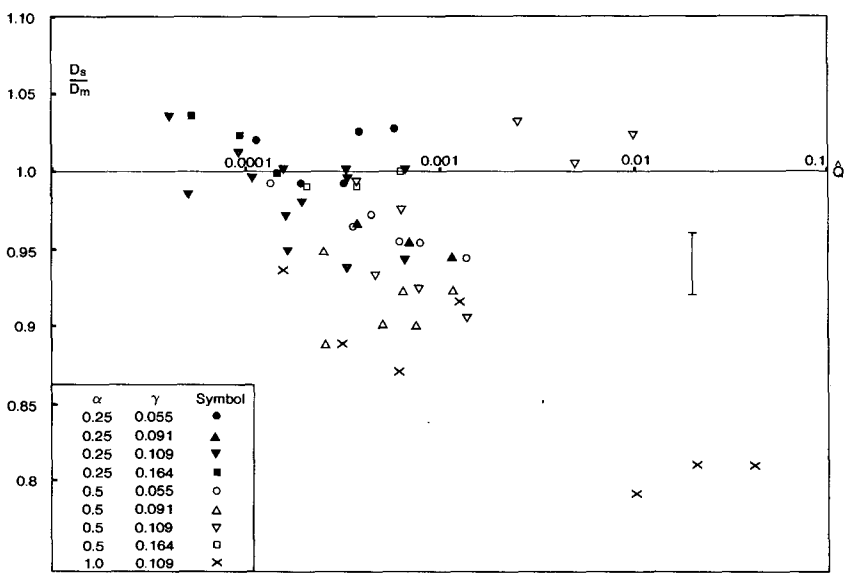


FIG. 7. Observed values of the depth of the fluid $D_s$ at the point of separation from the boundary, expressed in terms of $D_m$, the mean depth of fluid at the exit (used here as an approximation to the flow-weighted mean depth $\overline{D_e}$), for a range of values of $\hat{Q}$, $\alpha$, and $\gamma$.

current, with the effect that the initially narrow current appears to broaden substantially in this region and then resume its original thickness when it emerges from this region farther downstream. Although the visualization technique of dyed fluid in the current contributes to this picture because slow-moving or stationary fluid remains in place and appears to be part of the current, video images of these flows do show that the net effect is to produce a slower current in the mean in this region.

## 6. Conclusions

We have described qualitative and quantitative observations of an experimental realization of a barotropic western boundary current, its separation from the boundary, and its subsequent meandering as a free inertial jet. The properties of this current have been described in terms of the familiar dynamical concepts of conservation of potential vorticity and the Bernoulli equation. In the inviscid model of the attached boundary current, as one moves downstream and the mean depth decreases, the relative vorticity becomes anticyclonic, the speed at the boundary increases and the pressure there decreases.

This inviscid model has been corrected to satisfy the no-slip boundary condition on the sidewall, giving rise (we believe) to a new form of sidewall boundary layer in rotating fluids. This sidewall boundary layer in the attached current described in section 4b has a thickness $\delta$ that is dependent on the magnitude of the downstream pressure gradient. Specifically,

$$\delta = \left( \frac{\nu D_0}{d(D_0 v_I)/dy)} \right)^{1/2}, \qquad (6.1)$$

where $D_0$ and $v_I$ denote, respectively, the depth and inviscid velocity at the wall.

The process of separation of the current from the boundary has been shown to be due to the establishment of a minimum pressure value at the downstream end of the tank, which sets the minimum value in the current. Since the pressure in a current that remained attached to the boundary would fall below this value, separation occurs to prevent it. Hence, this separation may be viewed as being caused by the current moving into a region of adverse pressure gradient, which is the familiar mechanism that causes separation in viscous boundary layers in conventional fluid dynamics. A weak circulation is observed in the downstream region, with flow along the boundary toward the separation point.

The separated current is observed to contain meanders about a mean direction, initiated at the point of separation. Its behavior is, in general, consistent with the theory of Robinson and Niiler (1967), with the exception of small-scale features in the experiment that are attributed to the instability of the current.

What is the relevance of these results for the ocean? Although this model is barotropic, the same dynamical principles apply to the ocean if suitable account is taken of the vertical density structure. Attached western boundary currents are situated over continental slopes and are substantially barotropic, in that they "feel" the local bottom. The mechanism of separation due to a downstream-imposed pressure gradient, as experienced by a current with given structure, is clearly still valid and is conceptually useful in identifying the cause of separation. The downstream source of this mechanism has yet to be identified in any given case. After separating, the meandering current is clearly baroclinic but again the same principles apply with variations.

*Acknowledgments.* The authors are grateful to David Murray for his consistently expert assistence with the experiments.

REFERENCES

Baines, P. G., and H. Mitsudera, 1994: On the mechanism of shear flow instabilities. *J. Fluid Mech.*, **276,** 327–342.

Batchelor, G. K., 1967: *An Introduction to Fluid Dynamics.* Cambridge University Press, 615 pp.

Fofonoff, N. P., 1981: The Gulf Stream system. *Evolution of Physical Oceanography,* B. Warren and C. Wunsch, Eds., The MIT Press, 112–139.

Gill, A. E., 1982: *Atmosphere–Ocean Dynamics.* Academic Press, 662 pp.

Greenspan, H. P., 1968: *The Theory of Rotating Fluids.* Cambridge University Press, 327 pp.

Haidvogel, D. B., J. C. McWilliams, and P. R. Gent, 1992: Boundary current separation in a quasigeostrophic, eddy-resolving ocean circulation model. *J. Phys. Oceanogr.*, **22,** 882–902.

Hughes, R. L., 1985: On inertial currents over a sloping continental shelf. *Dyn. Atmos. Oceans,* **9,** 49–73.

——, 1986: On the role of criticality in coastal flows over irregular bottom topography. *Dyn. Atmos. Oceans,* **10,** 129–147.

——, 1993: A frictional sublayer for western boundary currents. *Dyn. Atmos. Oceans,* **17,** 243–256.

Leetmaa, A., and A. F. Bunker, 1978: Updated charts of the mean annual wind stress, convergence in the Ekman layers and Sverdrup transports in the North Atlantic. *J. Mar. Res.*, **36,** 311–322.

Morton, B. R., 1984: The generation and decay of vorticity. *Geophys. Astrophys. Fluid Dyn.*, **28,** 277–308.

Parsons, A. T., 1969: A two-layer model of Gulf Stream separation. *J. Fluid Mech.*, **39,** 511–528.

Pedlosky, J., 1987: On Parsons' model of the ocean circulation. *J. Phys. Oceanogr.*, **17,** 1571–1582.

Robinson, A. R., and P. P. Niiler, 1967: The theory of free inertial currents. I. Path and structure. *Tellus,* **19,** 269–291.

Stommel, H. M., 1965: *The Gulf Stream: A Physical and Dynamical Description.* University of California Press, 248 pp.

Veronis, G., 1973: Model of world ocean circulation. I. Wind-driven, two-layer. *J. Mar. Res.*, **31,** 228–288.

——, 1981: Dynamics of large-scale ocean circulation. *Evolution of Physical Oceanography,* B. Warren and C. Wunsch, Eds., The MIT Press, 140–183.

Verron, J., and C. Le Provost, 1991: Response of eddy-resolved general circulation numerical models to asymmetrical wind forcing. *Dyn. Atmos. Oceans,* **15,** 505–534.